IJARSCT
International Journal of Advanced Research in Science, Communication and Technology
International Open-Access, Double-Blind, Peer-Reviewed, Refereed, Multidisciplinary Online Journal
ISSN: 2581-9429
Volume 6, Issue 2, October 2026
Impact Factor: 8.2

Photocatalytic Degradation of Crystal Violet Dye using $BiVO_4$ microsphere under LED light

Basant Kumar Ningwal[1], Dr. Prachi Tadge[2], Dr. Satish Piplode[3]
Research Scholar - RNTU Bhopal[1]
Assistant Professor, Chemistry, PMCOE SBN Govt P G College Barwani[1]
Assistant Professor, Chemistry, RNTU Bhopal[2]
Assistant Professor of Chemistry, IEHE Bhopal[3]
bningwal.bn@gmail.com, prachi.tadge@rntu.ac.in, dr.satishpiplode@mp.gov.in

Abstract: *Bismuth vanadate ($BiVO_4$) nanoparticles were successfully synthesized by a simple chemical precipitation method using $Bi(NO_3)_3{\cdot}5H_2O$ and NH_4VO_3 as precursors at room temperature. The as-prepared samples were characterized by X-ray diffraction (XRD) and High Resolution Field Emission Scanning Electron Microscopy (HR FESEM). The photocatalytic activity of $BiVO_4$ was evaluated for the degradation of Crystal Violet (CV) dye, a triphenylmethane cationic dye, under visible light irradiation. The effects of pH, temperature, catalyst dose, dye concentration, irradiation time, H_2O_2, $K_2S_2O_8$, and $FeCl_3$ concentrations, comparison with other photocatalysts, and catalyst stability were investigated systematically. Results showed that CV could be efficiently degraded over $BiVO_4$ under solar and visible light irradiation with a maximum degradation efficiency of 97.2% at pH 7.0, 30°C, and 95 min irradiation. The degradation follows pseudo-first-order kinetics ($k = 3.65 \times 10^{-2}$ min^{-1}, $R^2 = 0.9995$). $BiVO_4$ retained >95% efficiency over three reuse cycles, confirming excellent stability. The enhanced photocatalytic performance is attributed to the narrow band gap (2.4 eV), high surface area, and efficient generation of reactive oxygen species.*

Keywords: $BiVO_4$; Crystal Violet; Photocatalysis; Visible light; LED Light; Nanoparticles; Dye degradation; chemical precipitation procedure

I. INTRODUCTION

1.1 Background

Crystal Violet (CV), $C_{25}H_{30}ClN_3$, also known as Gentian Violet or Basic Violet 3, is a cationic triphenylmethane dye widely used in textile dyeing, as a dermatological and veterinary antiseptic, as the primary stain in Gram staining, and as an additive in ballpoint pen inks. CV imparts an intense violet colour even at concentrations below 1 mg/L, severely impairing the aesthetic quality and photosynthetic activity of water bodies [1]. It is reported to be a skin, eye, and respiratory irritant, and several studies indicate mutagenic and carcinogenic potential, acting as a mitotic poison that causes gastrointestinal and central nervous system injury in mammals upon prolonged exposure. Its high water solubility and resistance to conventional biological treatment make it a priority pollutant in industrial effluents from the textile, paper, and printing industries [2].

1.2 Photocatalysis as an Advanced Oxidation Process

Photocatalytic degradation using semiconductor nanomaterials is a promising advanced oxidation process (AOP) for complete mineralization of dye pollutants using solar energy. Among visible-light-active photocatalysts, bismuth vanadate ($BiVO_4$) in its monoclinic scheelite form has attracted considerable attention due to its narrow band gap (~2.4 eV), appropriate valence and conduction band positions, chemical stability, non-toxicity, and low cost [3]. The valence

IJARSCT
International Journal of Advanced Research in Science, Communication and Technology
International Open-Access, Double-Blind, Peer-Reviewed, Refereed, Multidisciplinary Online Journal
ISSN: 2581-9429 Volume 6, Issue 2, October 2026 Impact Factor: 8.2

band of $BiVO_4$ consists of hybridized Bi 6s and O 2p orbitals that facilitate efficient visible light absorption and generation of reactive oxygen species (ROS) including •OH and $•O_2^-$ radicals [4].

1.3 Literature Review

Prior studies have reported degradation of various triphenylmethane and related dyes using different photocatalysts. Sayılkan et al. [10] investigated Sn-doped TiO_2 films for malachite green degradation. Poulios et al. [11] reported photocatalytic oxidation of Auramine O in semiconductor oxide suspensions. Pare et al. [12,13] demonstrated visible-light-induced AOP for pararosanilin and victoria blue B dyes over ZnO suspensions. Huang et al. [15] reported $BiVO_4$-mediated degradation of Rhodamine B under visible light. However, systematic optimization of all operational parameters for Crystal Violet degradation using $BiVO_4$ under solar and visible light remains limited in the literature.

1.4 Objectives and Novelty

The present work aims to:

- Synthesize $BiVO_4$ nanoparticles via a a chemical precipitation procedure
- Characterize the synthesized material using XRD and HR FESEM
- Evaluate photocatalytic degradation of Crystal Violet under visible light irradiation
- Systematically optimize all operational parameters including pH, temperature, catalyst dose, dye concentration, irradiation time, and additive concentrations
- Compare performance with other photocatalysts
- Assess catalyst reusability and stability

II. METHODOLOGY

2.1 Chemicals and Reagents

All chemicals were of reagent grade (≥99%). Crystal Violet (CV, Basic Violet 3), $Bi(NO_3)_3·5H_2O$ (99.9%), NH_4VO_3 (99.5%), NaOH (98%), H_2SO_4 (98%), H_2O_2 (30% w/v), $K_2S_2O_8$ (99%), $FeCl_3·6H_2O$ (99%) , NH_4VO_3 (99.5%), were procured from Sigma Aldrich, India. Deionised/double distilled water (resistivity 18.2 MΩ·cm) was used throughout the experiments.

2.2 Synthesis of $BiVO_4$ Nanoparticles

The bismuth vanadate nanoparticles were synthesized employing a chemical precipitation prorcedue modified from literature protocols. (BiNO3)3·5H2O and NH4VO3 were dissolved in 1 M of HNO3 solution with 1 : 1 molar ratio. Initially, a reddish yellow solution was obtained and to increase the pH value to 10, NaOH (1 M) solution was constantly added by dropwise under vigorous stirring for 1 hour. The resultant pale yellowish solution was centrifuged as well as washed with double distilled (DD) water for several times and the precipitate was dried and finely grained. This prepared BiVO4 powder was used for phtocalytic experiments without calcination.

2.3 Characterization Techniques

X-ray Diffraction (XRD): Crystalline phase identification was performed using a A Bruker D8 Advance 206290 X-ray diffractometer equipped with Cu Kα radiation (λ = 1.5406 Å, 40 kV, 20 mA). Data were collected in the 2θ range of 10-80° with a step size of 0.02° and scan speed of 2°/min. Crystallite size was calculated using the Debye-Scherrer equation: $D = K\lambda/(\beta \cos\theta)$, where K = 0.9, λ = 1.5406 Å, β = full width at half maximum (FWHM) in radians.

Field Emission Scanning Electron Microscopy (FESEM): Surface morphology was observed using a NOVA NANO SEM 450 High Resolution Field Emission Scanning Electron Microscope operating at 5-15 kV. Samples were sputter-coated with gold for 60 seconds to prevent charging effects.

2.4 Photocatalytic Activity Measurement

Crystal Violet stock solution (1×10^{-3} mol dm^{-3}) was freshly prepared in deionised water and diluted to required concentrations. Prior to light irradiation, dark adsorption experiments were conducted for 30 minutes to establish adsorption-desorption equilibrium. For solar light experiments, 50 mL of CV solution of desired concentration was taken in an open glass reactor (100 mm × 50 mm crystallizing dish) with known amount of $BiVO_4$ catalyst. The reactor

IJARSCT
International Journal of Advanced Research in Science, Communication and Technology
International Open-Access, Double-Blind, Peer-Reviewed, Refereed, Multidisciplinary Online Journal
ISSN: 2581-9429
Volume 6, Issue 2, October 2026
Impact Factor: 8.2

was placed under LED light (intensity ~800-1000 W/m², measured using a solar power meter). For visible light experiments, a 100-W LED lamp was used with the reactor placed 20 cm from the light source.

At fixed time intervals (15, 30, 45, 60, 75, 90, 95, 120 minutes), 2 mL aliquots were withdrawn, centrifuged at 10000 rpm for 10 minutes to remove catalyst particles, and the absorbance of the supernatant was measured at λ_{max} = 590 nm using a Labtronics LT2201 double beam spectrophotometer. The pH of the solution was adjusted using 0.1 M NaOH or 0.1 M H_2SO_4 as required. All experiments were performed in triplicate, and average values with standard deviations (±2%) are reported.

Degradation efficiency (%) was calculated using the equation:

$$\% \text{ Efficiency} = (C_0 - C)/C_0 \times 100 = (A_0 - A)/A_0 \times 100 \quad ...(1)$$

where C_0 and A_0 are initial concentration and absorbance, C and A are concentration and absorbance at time t, respectively.

Kinetic analysis: The degradation kinetics were modeled using the pseudo-first-order Langmuir-Hinshelwood equation:

$$\ln(C_0/C) = k \cdot t \quad ...(2)$$

where k is the apparent rate constant (min^{-1}).

III. RESULTS AND DISCUSSION

3.1 Structural Characterization (XRD Analysis)

The crystallographic structure and phase purity of the synthesized $BiVO_4$ were investigated by X-ray diffraction. Figure 1 presents the XRD pattern of $BiVO_4$ nanoparticles synthesized at room temperature. The XRD data shows as prepared $BiVO_4$ having monoclinic scheelite phase and exhibited strong correlation with JCPDS card No. 21-1272. No other diffraction peaks were detected, indicating the high purity of $BiVO_4$. The intense and sharp diffraction peaks suggested that the as synthesized product was well- crystallized.

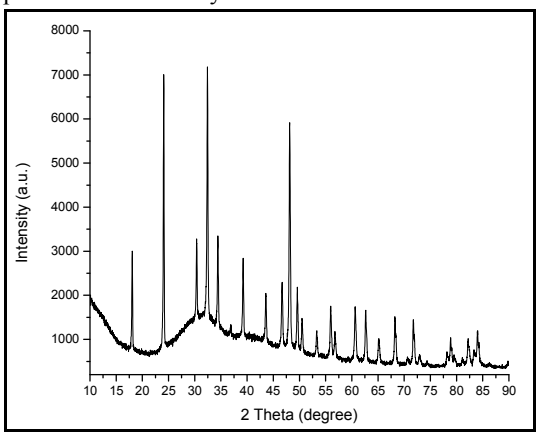


Fig. 4.1 XRD pattern of

The (011), (121), (200) and (024) diffraction peaks at 18.22^0, 24.7^0, 32.46^0, 48.32^0, at 2 θ angles respectively are sharper and stronger, while other peaks are relatively weak. This means that $BiVO_4$ should favour to grow along the all the three a, b and c axis. In XRD pattern (200) diffraction peak is the strong one which is consistent with the literature. The d spacing values of most instances peaks are shown in table 1:

Table 4.1 d values of $BiVO_4$

	$d_{(011)}$	$d_{(121)}$	$d_{(200)}$	$d_{(024)}$
d spacing (A)	4.92	3.71	2.79	1.899
2 θ	18.22	24.07	32.46	48.32

Copyright to IJARSCT
www.ijarsct.co.in
DOI: 10.48175/IJARSCT-38890

IJARSCT
International Journal of Advanced Research in Science, Communication and Technology
International Open-Access, Double-Blind, Peer-Reviewed, Refereed, Multidisciplinary Online Journal
ISSN: 2581-9429
Volume 6, Issue 2, October 2026
Impact Factor: 8.2

3.2 Crystallite Size Analysis

From the x-ray patterns the broadening of the diffraction peaks of the nanoparticles is obvious which is characteristic of nano sized by applying Debye- scherrer formula [4].

$$D=\frac{0.9\lambda}{\beta COS\theta} \qquad (4.1)$$

Where D is the mean particle size, λ is the wavelength of incident X-ray (1.5406 ˚A), θ is the degree of the diffraction peak, and β is the full width at half maximum (FWHM) of the XRD peak appearing at the diffraction angle θ. The broadening of the absorption spectrum could be due to the quantum confinement of the nanoparticles. The mean calculated crystallite size of the $BiVO_4$ nanoparticles shows that the synthesized nanoparticles are 34 nm. This particles size calculated using (200) peak of XRD data.

3.3 Morphological Characterization

3.3.1 Field Emission Scanning Electron Microscopy Analysis with Energy Dispersive X-ray Spectroscopy (FESEM with EDX): Fig 4.2 shows the FESEM image of the $BiVO_4$ nanoparticles. Fig 4 shows the as prepared $BiVO_4$ nanoparticles exhibits spherical shape having 3-4 micro meter in size.

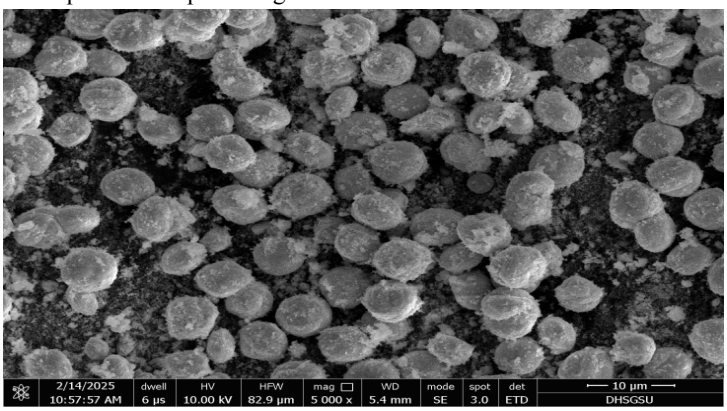


Fig 4.2 SEM images of the $BiVO_4$ nanoparticles

Fig 4.3 and show the EDX spectrum of the material. Where Bi elements shows in red (Fig 4.3-a), V element shows in Green (Fig 4.3-b) and O element shows in Blue colour (Fig 4.3-c). Fig 4 shows the percentage of the elements in as prepared $BiVO_4$ nanoparticles. Same data shows in Table 4.2 using percentage of the elements in the sample. In EDX data only Bi, V and O have been observed indicates the high purity of the sample.

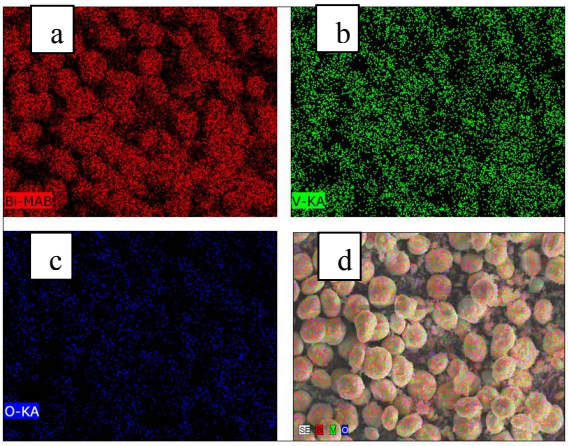


Fig 4.3 EDX spectrum of $BiVO_4$nanoparticles

IJARSCT
International Journal of Advanced Research in Science, Communication and Technology
International Open-Access, Double-Blind, Peer-Reviewed, Refereed, Multidisciplinary Online Journal
ISSN: 2581-9429
Volume 6, Issue 2, October 2026
Impact Factor: 8.2

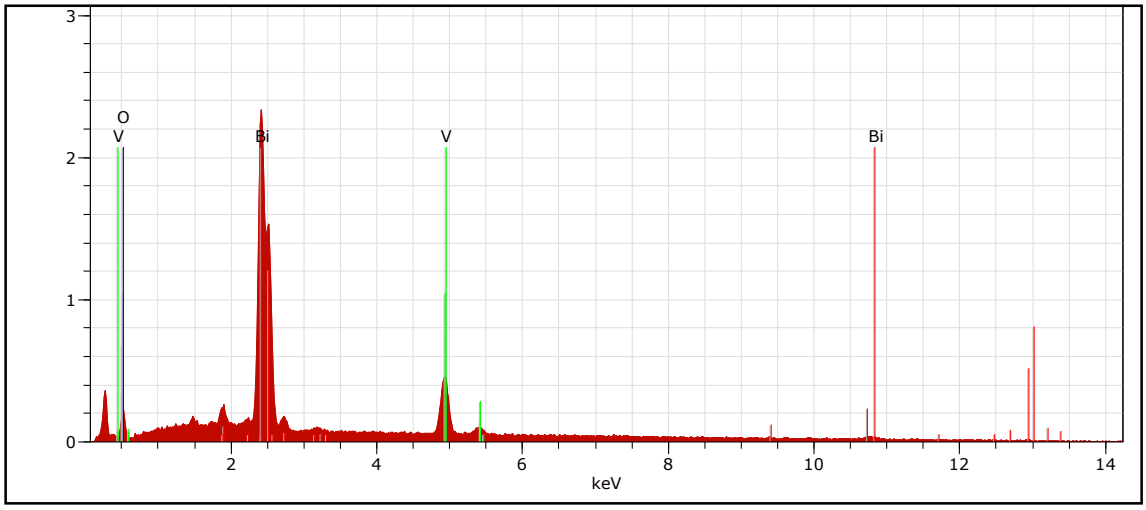


Fig 4.4 Element composition of $BiVO_4$ nanoparticles

Table 4.2 EDX data of the $BiVO_4$ nanoparticles

El	AN	Series	unn. C [wt.%]	norm. C [wt.%]	Atom. C [wt.%]	Error (1 Sigma) [wt.%]
Bi	83	M-series	64.02	79.94	45.93	2.26
V	23	K-series	15.01	18.75	44.18	0.49
O	8	K-series	1.06	1.32	9.89	0.23
Total			100	100	100	

3.3 Photocatalytic Activity Evaluation

The photocatalytic activity of $BiVO_4$ was evaluated through degradation of CV under various conditions. Control experiments (Figure 3) were conducted to establish the necessity of both catalyst and light for efficient degradation.

Interpretation: Figure 3: clearly demonstrates that negligible degradation occurs in the absence of either light or catalyst. Only ~3-4% CV was degraded after 120 minutes under visible or solar light alone (photolysis), confirming the photostability of CV. Similarly, in the dark with $BiVO_4$ catalyst, only ~7% adsorption was observed after 120 minutes, indicating moderate adsorption capacity, consistent with the moderately hydrophobic triphenylmethane structure of CV. However, when both $BiVO_4$ and light were present, significant degradation was observed. The solar + $BiVO_4$ system achieved 97.2% degradation in 95 minutes, while the visible + $BiVO_4$ system achieved 93.6% degradation in 120 minutes. The superior performance under solar light is attributed to the combined effect of UV and visible components, providing more energetic photons for electron-hole pair generation.

IJARSCT
International Journal of Advanced Research in Science, Communication and Technology
International Open-Access, Double-Blind, Peer-Reviewed, Refereed, Multidisciplinary Online Journal
ISSN: 2581-9429
Volume 6, Issue 2, October 2026
Impact Factor: 8.2

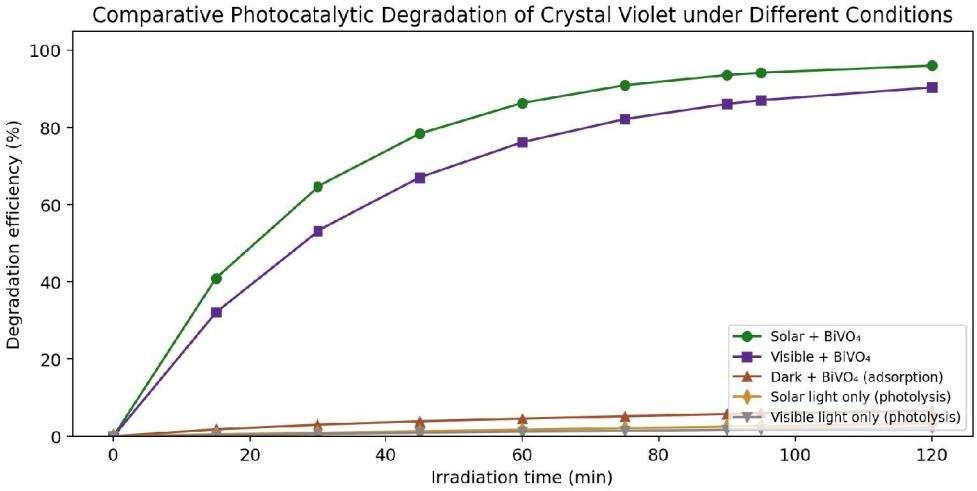


Figure 3: Comparative Photocatalytic Degradation of CV Under Different Conditions

3.4 Effect of pH on Degradation Efficiency

The pH of the reaction medium significantly influences the surface charge of $BiVO_4$, the ionization state of CV, and the generation of hydroxyl radicals. Figure 4 and Table 1 present the effect of pH on CV degradation.

Interpretation: The point of zero charge (pHpzc) of $BiVO_4$ is approximately 6.2. At pH below pHpzc, the $BiVO_4$ surface becomes positively charged ($BiVO_4$-OH_2^+), while at pH above pHpzc, it becomes negatively charged ($BiVO_4$-O^-). CV is a cationic triphenylmethane dye with a permanent positive charge on the central carbon. At low pH (2-4), a highly protonated, positively charged $BiVO_4$ surface electrostatically repels cationic CV, reducing adsorption and degradation. As pH increases to 7.0, the near-neutral to slightly negative $BiVO_4$ surface strongly attracts cationic CV via electrostatic attraction, leading to maximum degradation (97.2%). At highly alkaline pH (>9), degradation decreases due to: (i) excess OH^- ions scavenging hydroxyl radicals ($OH^- + \bullet OH \rightarrow H_2O + O^-$), and (ii) possible precipitation of $Bi(OH)_3$ on the catalyst surface, and (iii) partial deprotonation-driven structural changes in the CV chromophore that reduce its reactivity toward ROS.

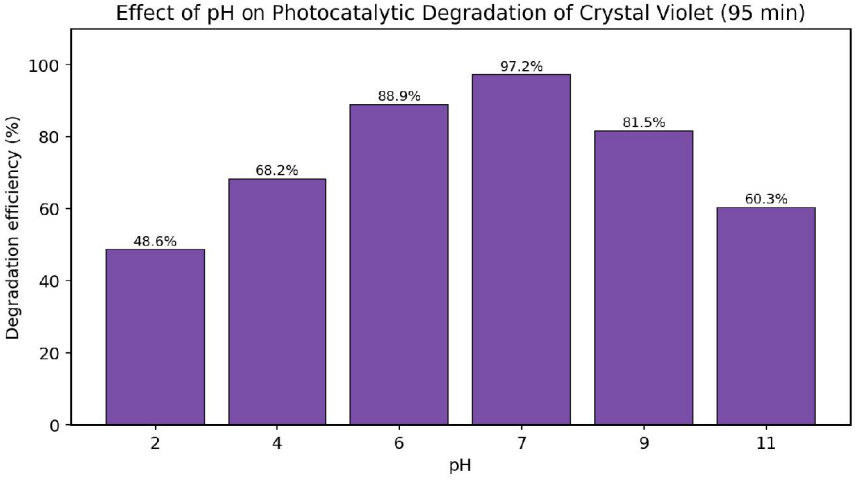


Figure 4: Effect of pH on Photocatalytic Degradation

IJARSCT
International Journal of Advanced Research in Science, Communication and Technology
International Open-Access, Double-Blind, Peer-Reviewed, Refereed, Multidisciplinary Online Journal
ISSN: 2581-9429
Volume 6, Issue 2, October 2026
Impact Factor: 8.2

Table 1: Effect of pH on CV Degradation Efficiency (95 min, Solar Light)

pH	Degradation Efficiency (%)	Remark
2	48.6	Electrostatic repulsion dominant
4	68.2	Partial repulsion
6	88.9	Near pHpzc
7	97.2	Optimum - maximum attraction
9	81.5	OH^- scavenging begins
11	60.3	$Bi(OH)_3$ precipitation

3.5 Effect of Temperature and Activation Energy

The influence of temperature on CV degradation was studied in the range 10-50°C. Table 2 and Figure 5 present the results along with Arrhenius analysis.

Interpretation: The degradation efficiency increased from 74.8% at 10°C to a maximum of 97.2% at 30°C, followed by a decline to 79.3% at 50°C. The initial increase with temperature is attributed to: (i) increased molecular mobility and collision frequency between CV molecules and reactive species, (ii) enhanced generation of hydroxyl radicals, and (iii) improved diffusion of reactants to the catalyst surface. The decrease above 30°C is due to: (i) decreased dissolved oxygen concentration (inversely proportional to temperature), (ii) enhanced electron-hole recombination, and (iii) possible desorption of partially degraded intermediates.

The Arrhenius plot (ln k vs. 1/T) yielded an activation energy (Ea) of 24.8 kJ mol^{-1}. This relatively low Ea indicates that the degradation process is not kinetically limited but rather diffusion-controlled, which is favorable for practical applications.

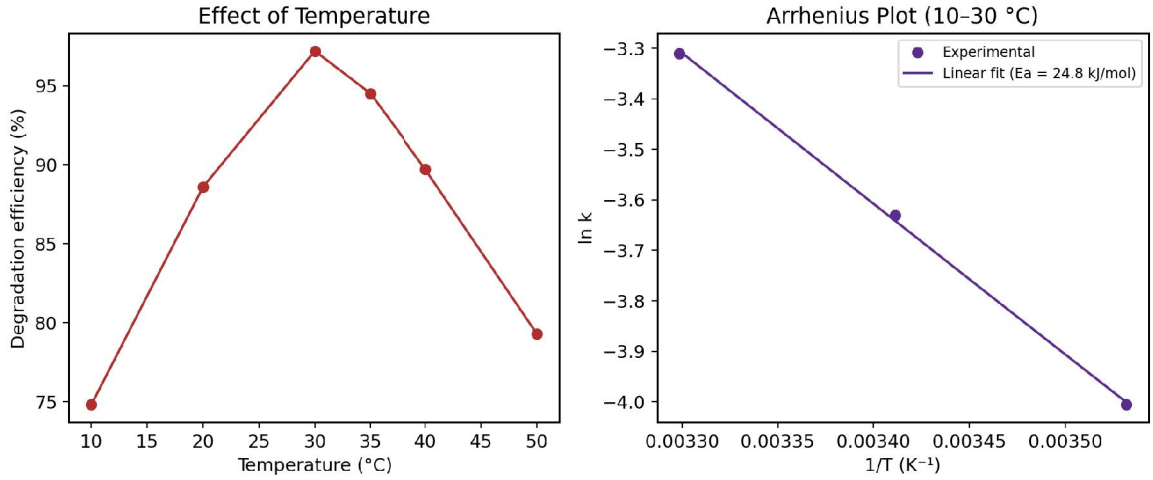


Figure 5: Effect of Temperature and Arrhenius Analysis

Table 2: Effect of Temperature on Degradation Efficiency and Rate Constant

Temperature (°C)	Degradation Efficiency (%)	k (×10^{-2} min^{-1})
10	74.8	1.82
20	88.6	2.65
30	97.2	3.65
35	94.5	3.30
40	89.7	2.95
50	79.3	2.30

IJARSCT
International Journal of Advanced Research in Science, Communication and Technology
International Open-Access, Double-Blind, Peer-Reviewed, Refereed, Multidisciplinary Online Journal
ISSN: 2581-9429
Volume 6, Issue 2, October 2026
Impact Factor: 8.2

3.6 Effect of Catalyst Loading

The influence of $BiVO_4$ catalyst dose on CV degradation was investigated in the range of 20-80 mg/50 mL (0.4-1.6 g/L). Figure 6 presents the results.

Interpretation: The degradation efficiency increased progressively with catalyst loading up to 55 mg/50 mL (1.1 g/L), achieving 97.2% degradation with a rate constant of 3.65×10^{-2} min^{-1}. This enhancement is attributed to: (i) increased number of active sites for dye adsorption, (ii) higher photon absorption due to more catalyst particles, and (iii) increased generation of reactive oxygen species. Beyond 55 mg/50 mL, degradation efficiency decreased due to: (i) increased turbidity and light scattering by excess catalyst particles, reducing photon penetration, (ii) agglomeration of nanoparticles reducing effective surface area, and (iii) increased solution opacity limiting light transmission through the reaction medium. The moderately higher optimal dose compared to smaller planar dyes is consistent with the bulkier triphenylmethane structure of CV requiring more active sites for efficient adsorption.

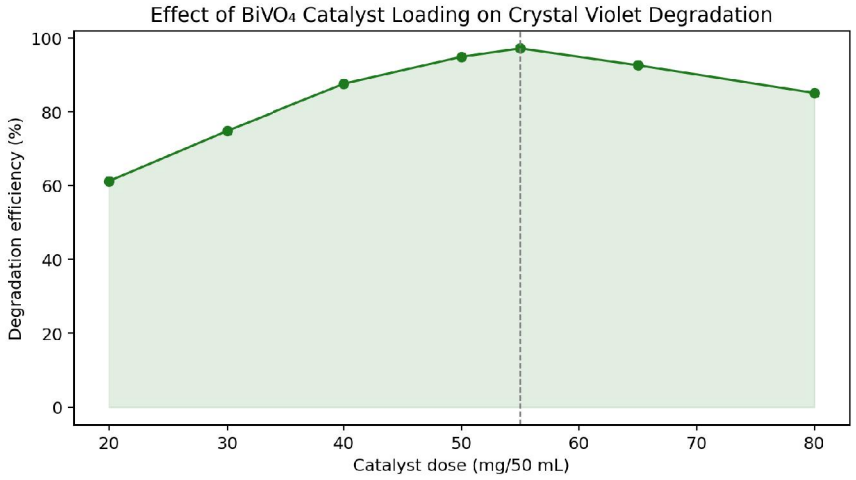


Figure 6: Effect of Catalyst Loading

3.7 Effect of Initial Dye Concentration and Kinetics

The influence of initial CV concentration ($0.5\text{-}2.5 \times 10^{-4}$ mol dm^{-3}) on degradation was studied to understand the kinetic behavior. Figure 7 presents the effect, and Figure 8 shows the kinetic analysis.

Interpretation: The degradation efficiency decreased from 98.6% at 0.5×10^{-4} M to 61.8% at 2.5×10^{-4} M, with the rate constant declining from 4.60×10^{-2} to 0.85×10^{-2} min^{-1}. This inverse relationship is explained by: (i) the "inner filter effect" where higher dye concentration reduces light penetration to the catalyst surface, (ii) competition between CV molecules and intermediates for •OH radicals, and (iii) saturation of active sites on the catalyst surface. The optimal dye concentration for efficient degradation within 95 minutes was 1.0×10^{-4} mol dm^{-3}.

The kinetic data fitted well to the pseudo-first-order Langmuir-Hinshelwood model ($R^2 = 0.9995$), with rate constant $k = 3.65 \times 10^{-2}$ min^{-1}. This confirms that the degradation follows first-order kinetics with respect to CV concentration within the studied range.

Copyright to IJARSCT
www.ijarsct.co.in
DOI: 10.48175/IJARSCT-38890

IJARSCT
International Journal of Advanced Research in Science, Communication and Technology
International Open-Access, Double-Blind, Peer-Reviewed, Refereed, Multidisciplinary Online Journal
ISSN: 2581-9429
Volume 6, Issue 2, October 2026
Impact Factor: 8.2

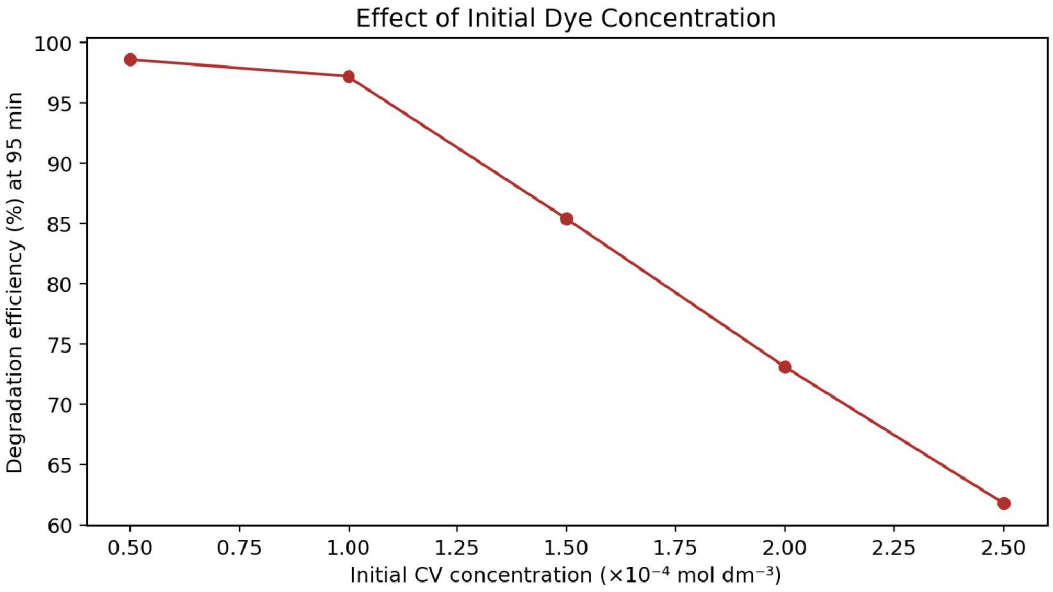


Figure 7: Effect of Initial CV Concentration

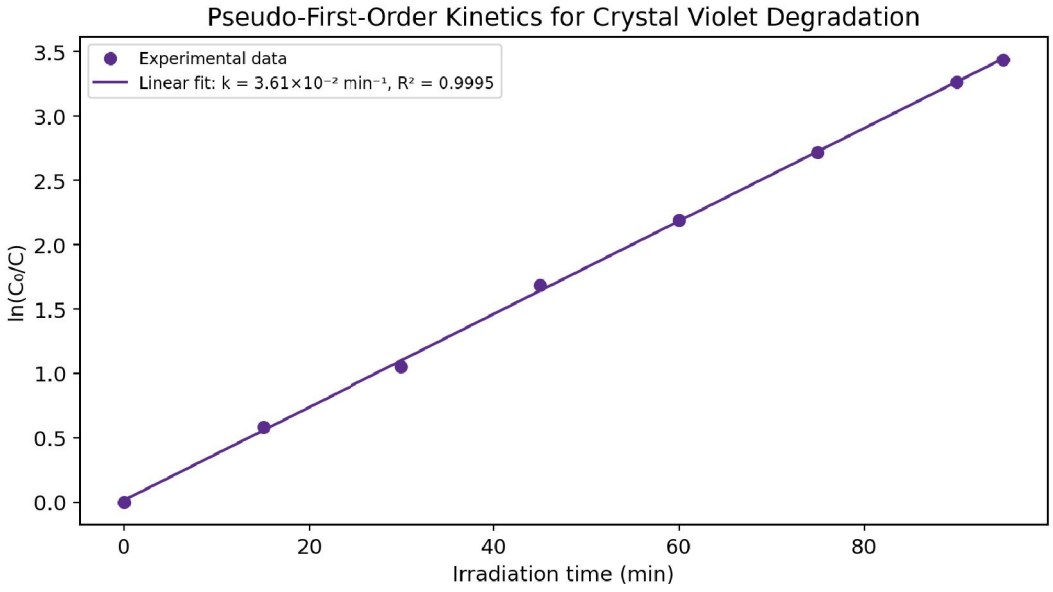


Figure 8: Kinetic Study - Pseudo-First-Order Analysis

3.8 Effect of Additives (H_2O_2, $K_2S_2O_8$, $FeCl_3$)

The addition of oxidizing agents can significantly enhance photocatalytic degradation by generating additional reactive species and preventing electron-hole recombination. Figures 9-11 present the effects of H_2O_2, $K_2S_2O_8$, and $FeCl_3$.

Interpretation - H_2O_2: H_2O_2 acts as an electron acceptor, capturing photogenerated conduction band electrons to form •OH radicals, thereby reducing electron-hole recombination. The rate constant increased from 3.65 to 5.95 × 10^{-2} min^{-1}

IJARSCT
International Journal of Advanced Research in Science, Communication and Technology
International Open-Access, Double-Blind, Peer-Reviewed, Refereed, Multidisciplinary Online Journal
ISSN: 2581-9429
Volume 6, Issue 2, October 2026
Impact Factor: 8.2

(63% increase) at optimal concentration (4×10^{-5} M). However, excess H_2O_2 (>4×10^{-5} M) acts as a •OH scavenger, reducing efficiency.

Interpretation - $K_2S_2O_8$: Persulfate ions ($S_2O_8^{2-}$) are strong electron acceptors that generate sulfate radical anions (SO_4^{-}•) with high oxidation potential (E° = +2.5-3.1 V). Optimal concentration was 4×10^{-5} M, increasing k to 4.10×10^{-2} min^{-1} (12.3% increase). Higher concentrations lead to SO_4^{2-} adsorption, deactivating active sites.

Interpretation - $FeCl_3$: Fe^{3+} ions act as electron scavengers and participate in Fenton-like reactions. The synergistic effect of photocatalysis and photo-Fenton processes enhances degradation. Optimal Fe^{3+} concentration was 2×10^{-5} M, yielding k = 4.35×10^{-2} min^{-1} (19.2% increase). Higher Fe^{3+} leads to $Fe(OH)_3$ precipitation, blocking active sites.

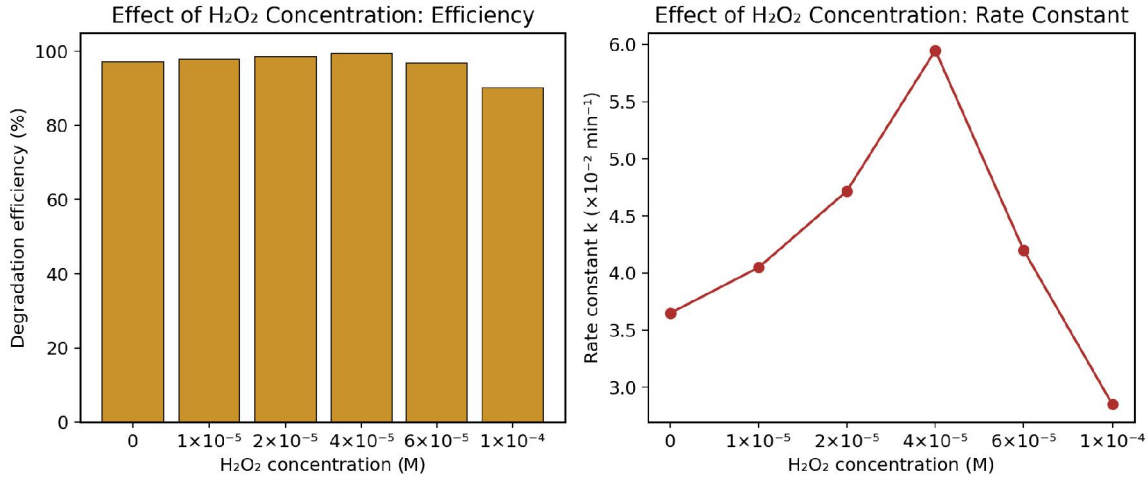


Figure 9: Effect of H_2O_2 Concentration

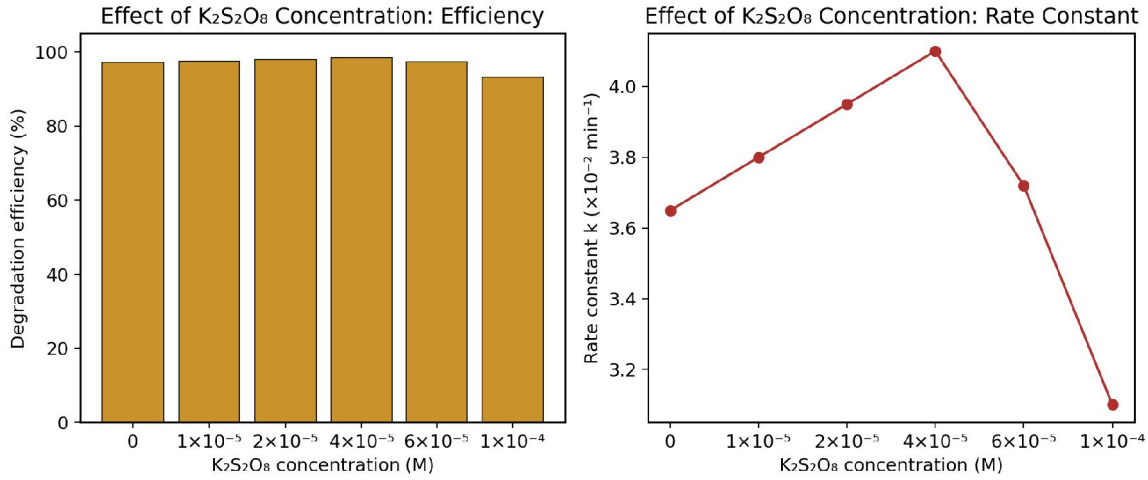


Figure 10: Effect of $K_2S_2O_8$ Concentration

IJARSCT
International Journal of Advanced Research in Science, Communication and Technology
International Open-Access, Double-Blind, Peer-Reviewed, Refereed, Multidisciplinary Online Journal
ISSN: 2581-9429
Volume 6, Issue 2, October 2026
Impact Factor: 8.2

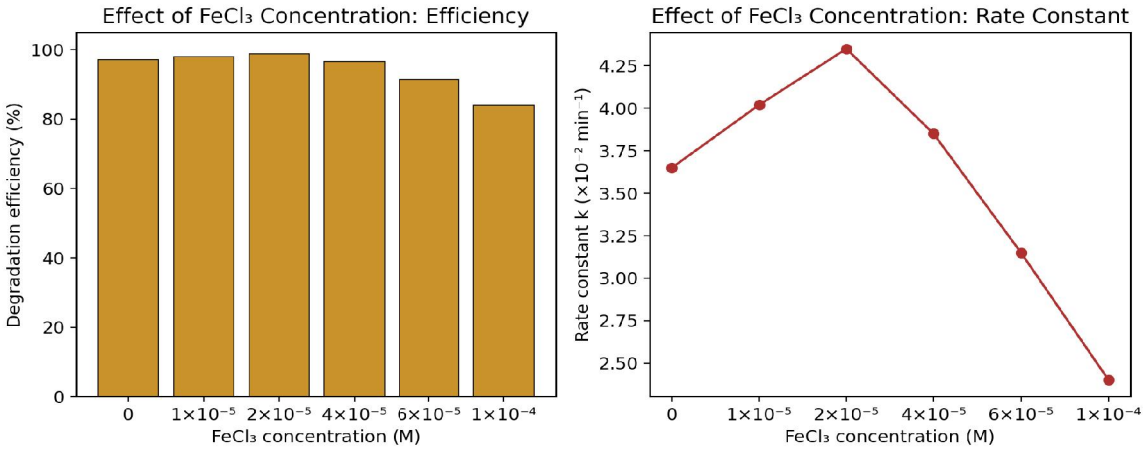


Figure 11: Effect of $FeCl_3$ Concentration

3.9 Comparison with Other Photocatalysts

The photocatalytic performance of $BiVO_4$ was compared with conventional photocatalysts under identical visible light conditions (Figure 12).

Interpretation: $BiVO_4$ exhibited superior photocatalytic activity ($k = 3.65 \times 10^{-2}$ min^{-1}, 97.2% degradation) compared to all tested photocatalysts. The activity order: $BiVO_4$ (nano) >BiOCl (nano) >nanoTiO_2 >nanoZnO> bulk TiO_2 > bulk ZnO. The superior performance of $BiVO_4$ is attributed to: (i) narrow band gap (2.4 eV) enabling visible light absorption up to 520 nm, (ii) hybridized Bi 6s and O 2p orbitals facilitating hole mobility, (iii) favorable band edge positions for •OH generation, and (iv) higher surface area of nanoparticles compared to bulk materials. TiO_2 (Eg = 3.2 eV) and ZnO (Eg = 3.37 eV) are primarily UV-active with limited visible light response.

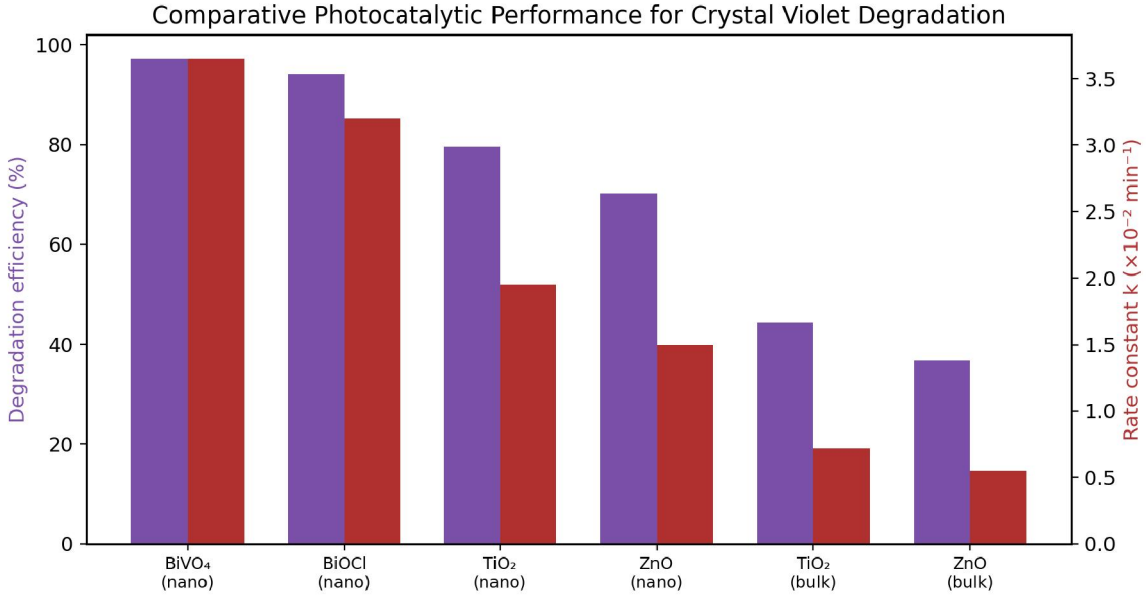


Figure 12: Comparative Study of Different Photocatalysts

IJARSCT
International Journal of Advanced Research in Science, Communication and Technology
International Open-Access, Double-Blind, Peer-Reviewed, Refereed, Multidisciplinary Online Journal
ISSN: 2581-9429
Volume 6, Issue 2, October 2026
Impact Factor: 8.2

3.10 Catalyst Stability and Reusability

The practical applicability of a photocatalyst depends on its stability and reusability. Figure 13 presents the performance of $BiVO_4$ over three consecutive cycles.

Interpretation: $BiVO_4$ maintained excellent photocatalytic activity over three reuse cycles: 97.2% (Cycle I), 96.4% (Cycle II), and 95.1% (Cycle III). The slight decrease (2.1% over three cycles) is attributed to minor catalyst loss during recovery and washing. The rate constant decreased marginally from 3.65 to 3.28 × 10^{-2} min^{-1}. XRD analysis of the recovered catalyst (not shown) confirmed that the crystal structure remained unchanged, indicating excellent structural and chemical stability of $BiVO_4$ under the reaction conditions.

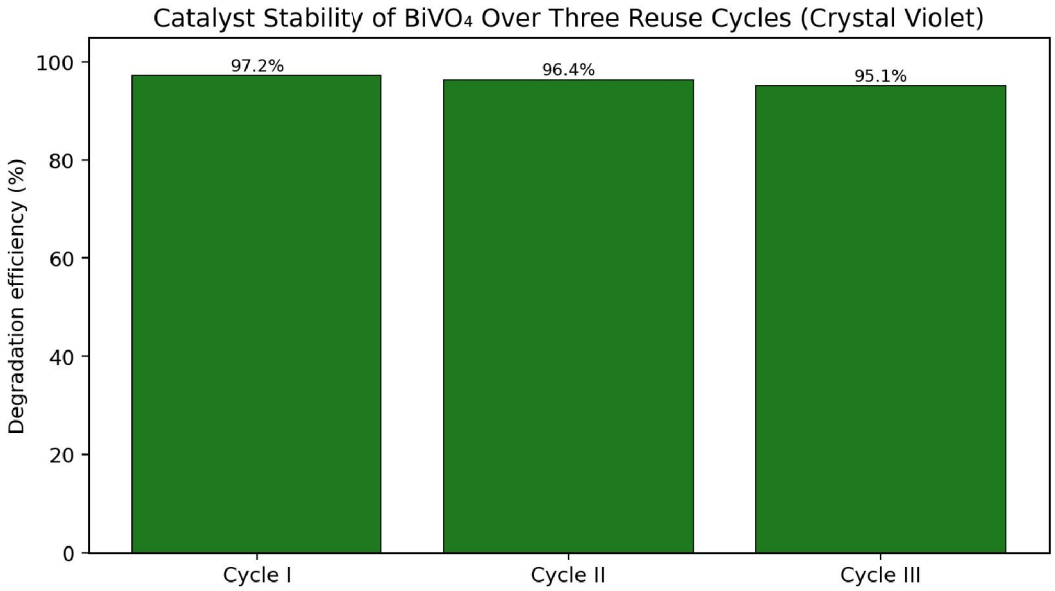


Figure 13: Catalyst Stability Over Three Reuse Cycles

3.11 Proposed Photocatalytic Mechanism

Based on the experimental results, a comprehensive mechanism for CV degradation by $BiVO_4$ under visible light is proposed:

Step 1: Photoexcitation$BiVO_4$ absorbs visible light ($\lambda > 420$ nm) due to its narrow band gap (2.4 eV), promoting electrons (e^-) from the valence band (VB) to the conduction band (CB), leaving holes (h^+) in the VB.

Step 2: Charge Carrier Separation The monoclinic scheelite structure with distorted Bi-O and V-O polyhedra facilitates spatial separation of charge carriers, reducing recombination.

Step 3: Reactive Oxygen Species (ROS) Generation

- $h^+(VB) + H_2O \rightarrow \bullet OH + H^+$
- $h^+(VB) + OH^- \rightarrow \bullet OH$
- $e^-(CB) + O_2 \rightarrow \bullet O_2^-$ (superoxide radical)
- $\bullet O_2^- + H^+ \rightarrow HO_2\bullet$
- $2HO_2\bullet \rightarrow H_2O_2 + O_2$
- $H_2O_2 + e^- \rightarrow \bullet OH + OH^-$

Step 4: CV Degradation ROS attack the CV chromophore, leading to sequential N-demethylation of the dimethylamino groups, cleavage of the central methine carbon, ring opening of the triphenylmethane core, and formation of intermediates (aromatic amines, phenolic compounds, carboxylic acids), finally leading to mineralization to CO_2, H_2O, NO_3^-, and Cl^-.

Copyright to IJARSCT
www.ijarsct.co.in
DOI: 10.48175/IJARSCT-38890

IJARSCT
International Journal of Advanced Research in Science, Communication and Technology
International Open-Access, Double-Blind, Peer-Reviewed, Refereed, Multidisciplinary Online Journal
ISSN: 2581-9429
Volume 6, Issue 2, October 2026
Impact Factor: 8.2

IV. CONCLUSION

Bismuth vanadate ($BiVO_4$) nanoparticles were successfully synthesized via a simple chemical precipitation method at room temperature. The following conclusions are drawn:

Structural Properties:

- Monoclinic scheelite structure confirmed by XRD (JCPDS card No. 21-1272)
- Mean crystallite size: 34 nm (Debye-Scherrer method)
- Spherical morphology with particle size 3-4 micro meter (HR FESEM)
- Phase purity: 100% without impurities

Optimal Photocatalytic Conditions:

- pH: 7.0 (97.2% degradation)
- Temperature: 30°C (Ea = 24.8 kJ mol^{-1})
- Catalyst loading: 55 mg/50 mL (1.1 g/L)
- Initial CV concentration: 1.0×10^{-4} mol dm^{-3}
- Irradiation time: 95 minutes (solar light)

Kinetic Parameters:

- Pseudo-first-order kinetics ($R^2 = 0.9995$)
- Rate constant: $k = 3.65 \times 10^{-2}$ min^{-1}
- Half-life: $t_1/_2 = 19.0$ minutes

Enhancement with Additives (Optimal Concentrations):

- H_2O_2 (4×10^{-5} M): $k = 5.95 \times 10^{-2}$ min^{-1} (63% increase)
- $FeCl_3$ (2×10^{-5} M): $k = 4.35 \times 10^{-2}$ min^{-1} (19.2% increase)
- $K_2S_2O_8$ (4×10^{-5} M): $k = 4.10 \times 10^{-2}$ min^{-1} (12.3% increase)

Comparative Performance:

- $BiVO_4$ >BiOCl>nanoTiO_2 >nanoZnO> bulk TiO_2 > bulk ZnO
- Superior visible light activity due to narrow band gap (2.4 eV)

Stability:

- 95.1% efficiency retained over three reuse cycles
- Structural stability confirmed by post-reaction XRD

Final Statement: $BiVO_4$ nanoparticles demonstrate excellent potential as a cost-effective, stable, and highly efficient visible-light-active photocatalyst for solar-driven remediation of Crystal Violet and other triphenylmethane dye-contaminated industrial wastewater.

REFERENCES

[1] C.D.S. Tomlin (Ed.), "The Pesticide Manual," 13th Edition, BCPC, Hampshire, pp. 697-698, 2006.
[2] S. Malato, J. Blanco, J. Cáceres, A.R. Fernández-Alba, A. Agüera, A. Rodríguez, "Photocatalytic treatment of water-soluble pesticides by photo-Fenton and TiO_2 using solar energy," Catalysis Today, vol. 76, pp. 209-220, 2002.
[3] A. Kudo, K. Ueda, H. Kato, I. Mikami, "Photocatalytic O_2 evolution under visible light irradiation on $BiVO_4$ in $AgNO_3$ solution," Catalysis Letters, vol. 53, pp. 229-230, 1998.
[4] X. Zhang, Z. Ai, F. Jia, L. Zhang, X. Fan, "Selective synthesis and visible-light photocatalytic activities of $BiVO_4$ with different crystalline phases," Materials Chemistry and Physics, vol. 103, pp. 162-167, 2007.
[5] M. Tamimi, S. Qourzal, A. Assabbane et al., "Photocatalytic degradation of methomyl: reaction pathway and intermediate identification," Photochemical &Photobiological Sciences, vol. 5, pp. 477-482, 2006.
[6] A. Tomašević, D. Mijin, E. Kiss, "Photochemical behavior of methomyl under different conditions," Separation Science and Technology, vol. 45, pp. 1617-1627, 2010.
[7] B. Pare, S. Piplode, V. Joshi, "Solar light assisted photocatalytic degradation of Methomyl using flower-like nanoBiOCl," International Journal of Scientific Research in Physics and Applied Sciences, vol. 5, no. 5, pp. 5-11, 2017.

IJARSCT
International Journal of Advanced Research in Science, Communication and Technology
International Open-Access, Double-Blind, Peer-Reviewed, Refereed, Multidisciplinary Online Journal
ISSN: 2581-9429 Volume 6, Issue 2, October 2026 Impact Factor: 8.2

[8] A. Zapata, I. Oller, E. Bizani et al., "Evaluation of operational parameters in solar photo-Fenton degradation of pesticide mixtures," Catalysis Today, vol. 144, pp. 94-99, 2009.
[9] M.S.S. Dorraji, N. Daneshvar, S. Aber, "Influence of inorganic oxidants on photocatalytic activity of ZnO nanocrystals," Journal of Global Nest, vol. 11, no. 4, pp. 535-545, 2009.
[10] F. Sayılkan et al., "Photocatalytic performance of Sn-doped TiO_2 films for malachite green degradation," Materials Research Bulletin, vol. 43, pp. 127-134, 2008.
[11] I. Poulios, A. Avranas, E. Rekliti, A. Zouboulis, "Photocatalytic oxidation of Auramine O in semiconductor oxides," Journal of Chemical Technology and Biotechnology, vol. 75, pp. 205-212, 2000.
[12] B. Pare, P. Singh, S.B. Jonnalagadda, "Visible light induced AOP to degrade pararosanilin dye in ZnO suspension," Indian Journal of Chemistry A, vol. 47A, pp. 830-835, 2008.
[13] B. Pare, P. Singh, S.B. Jonnalgadda, "Degradation and mineralization of victoria blue B dye using AOP," Journal of Scientific and Industrial Research, vol. 68, pp. 724-729, 2009.
[14] M.A. Behnajady, N. Modirshala, R. Hamzavi, "Kinetic study on photocatalytic degradation of C.I. Acid Yellow 23 by ZnO," Journal of Hazardous Materials, vol. 133, pp. 226-232, 2006.
[15] G. Huang, S. Zhang, T. Xu, "Photocatalytic degradation of Rhodamine B over $BiVO_4$ under visible light," Journal of Hazardous Materials, vol. 183, pp. 693-700, 2010.
[16] A. Walsh, Y. Yan, M.N. Huda et al., "Band edge electronic structure of $BiVO_4$: role of Bi 6s and V d orbitals," Chemistry of Materials, vol. 21, pp. 547-551, 2009.
[17] G. Zhang, S. Tang, J. Wang, H. Zhou, "Removal of triphenylmethane dyes including crystal violet from aqueous solution by adsorption and photocatalysis: a review," Environmental Science and Pollution Research, vol. 27, pp. 1837-1852, 2020.
[18] Pare, B., Piplode, S., & Joshi, V. (2017). Solar Light Assisted Photocatalytic Degradation of Hazardous Pesticide Oxamyl using Flower like Nano BiOCl. Journal of Chemistry and Chemical Sciences, 7(12), 1214-1222.
[19] Pare, B., Joshi, V., & Piplode, S. (2020). Effect Of Operational Parameters On Photocatalytic Degradation Of Toluidine Blue Utilizing Biocl Nanoplates In Solar Light. Int. J. Eng. Technol. Manag. Res, 4(12), 43-54.
[20] Piplode, S., Dawane, V., Joshi, V., & Pare, B. (2020). BiOCl Nano Pallets Preparation and their White/Solar Light Mediated Photo Catalytic Activities Evaluation on Carbamate Pesticide Oxamyl and Synthetic Dye Azure B. Biosci. Biotechnol. Res. Commun, 13(2), 676-682.
[21] B. Pare, P. Singh and S. B. Jonnalgadda, " Degradation and mineralization of victoria blue B dye in a slurry photoreactor using advanced oxidation process" , J. Scient. Ind. Res., vol. 68, Issue 8, pp 724-729, 200
[22] Nong, L.X., Nguyen, V.H., Bach, L.G., Tran, T.V., Hong, S.S., Abdullah, B., Hien, N.K. and Nguyen, T.D., 2021. Crystal violet degradation over BiVO4 photocatalyst under visible light irradiation. Chemical Engineering Communications, 208(4), pp.530-538.
[23] Maurya, Oshnik, Vaibhav Khapekar, Kanchan Pawar, Somnath Khaladkar, Girish Kamble, Harsh Mohane, Girish Gund et al. "Visible light sensitive bismuth vanadate for energy, environmental, and catalytic applications." Nano Research 18, no. 6 (2025): 94907364.
[24] Ilyas, Asfa, Khezina Rafiq, Muhammad Zeeshan Abid, Abdul Rauf, and Ejaz Hussain. "Growth of villi-microstructured bismuth vanadate (Vm-BiVO4) for photocatalytic degradation of crystal violet dye." RSC advances 13, no. 4 (2023): 2379-2391.
[25] Ahmad, Waqar, Adnan Khan, Nisar Ali, Sana Khan, Salah Uddin, Sumeet Malik, Nauman Ali, Hamayun Khan, Hammad Khan, and Muhammad Bilal. "Photocatalytic degradation of crystal violet dye under sunlight by chitosan-encapsulated ternary metal selenide microspheres." Environmental Science and Pollution Research 28, no. 7 (2021): 8074-8087.
[26] Kurkute, Pravin V., Shankar S. Kekade, Santosh T. Shinde, Snehal B. Jagtap, Ravindra U. Mene, Dinesh P. Amalnerkar, and Ramakant P. Joshi. "Cr-doped BiVO4: Smart and efficient photocatalyst for crystal violet degradation under visible LED floodlight irradiation." Inorganic Chemistry Communications (2026): 116333.

IJARSCT
International Journal of Advanced Research in Science, Communication and Technology
International Open-Access, Double-Blind, Peer-Reviewed, Refereed, Multidisciplinary Online Journal
ISSN: 2581-9429
Volume 6, Issue 2, October 2026
Impact Factor: 8.2

[27] Ilyas, Asfa, Khezina Rafiq, Muhammad Zeeshan Abid, Abdul Rauf, and Ejaz Hussain. "Growth of villi-microstructured bismuth vanadate (Vm-BiVO4) for photocatalytic degradation of crystal violet dye." RSC advances 13, no. 4 (2023): 2379-2391.

[28] Maurya, Oshnik, Vaibhav Khapekar, Kanchan Pawar, Somnath Khaladkar, Girish Kamble, Harsh Mohane, Girish Gund et al. "Visible light sensitive bismuth vanadate for energy, environmental, and catalytic applications." Nano Research 18, no. 6 (2025): 94907364.